# Effect of Sunlight on Photovoltaics as Optical Wireless Communication Receivers

Sovan Das, Adrian Sparks, Enrique Poves, Stefan Videv, John Fakidis, and Harald Haas, *Fellow, IEEE*

***Abstract*—This paper explores the effects of sunlight on using a low-cost off-the-shelf silicon solar panel as an optical wireless communication (OWC) receiver. A receiver circuit structure has been proposed to maximize simultaneous energy harvesting and data communication performance. An equivalent circuit model of the solar panel for simultaneous energy harvesting and wireless optical communication is discussed. By using the solar panel model, the effects of varying sunlight conditions on the performance of the model as an OWC receiver are estimated. Furthermore, an experimental setup is developed to study the effects and verify the simulated estimations. The experimental setup consists of a 3.5 m wireless optical link with a full Transmission Control Protocol and Internet Protocol (TCP/IP) network stack. The system uses DC-biased optical orthogonal frequency division multiplexing (DCO-OFDM) to use the available communication bandwidth efficiently. A 940 nm low-cost off-the-shelf laser device along with an off-the-shelf off-axis-parabolic mirror is used as the transmitter. The maximum user throughput achieved over the air is 28.3 Mb/s while simultaneously harvesting energy using the maximum power point tracking (MPPT) technique. The peak power harvested with simultaneous communication is 4.5 W. The harvested energy is stored in a 38 Wh lithium-ion (Li-ion) battery.**

***Index Terms*—Optical Wireless Communication (OWC), photovoltaics, LiFi, solar cell, energy harvesting, orthogonal frequency division multiplexing (OFDM).**

## I. Introduction

THE first semiconductor-junction solar cell was made with copper and copper oxide by Wilhelm Hallwachs in 1904 [1]. Early silicon solar cells were used to power the Telstar communication satellite launched in 1962 and were developed further for use in terrestrial installations. Modern manufacturing techniques have made low-cost silicon solar cells readily available. This has prompted an investigation into their application in areas other than direct sunlight to electrical energy conversion. Solar cells can harvest electrical energy from electromagnetic radiation generated by lasers and light-emitting diodes (LEDs) as well as sunlight. More recently, there has been a growing interest in using solar cells that harvest indoor light to power electronic devices for the Internet-of-Things (IoT) [2]. Such photovoltaic (PV)-powered devices are attractive for use in smart homes, smart offices, and smart buildings. Also, with recent advancements in the lighting industry, indoor lighting is shifting to semiconductor based light sources such as LEDs and lasers. These are highly efficient, have a long lifetime, can produce any color of light, and can be used to simultaneously transmit data. LiFi is the bidirectional optical wireless communications (OWC) technology which includes all the networking mechanisms for transmitting data via LEDs and lasers in the visible or infrared (IR) part of the optical spectrum [3]. The encoded data is transmitted as a variation in the intensity of the light emitted by the source. The LED is envisioned to serve the dual purpose of illumination and communication. Long-distance optical communication using LEDs becomes challenging as the radiation is spatially and temporally non-coherent. On the contrary, the radiation from lasers is coherent and has a significantly higher coherence length than LEDs. Therefore, lasers are used in long-distance wireless optical communication systems. In telecommunication, there are two laser structures that are commonly used: edge-emitting lasers and vertical-cavity surface-emitting lasers (VCSEL). Two important aspects of VCSEL are the low beam divergence and the symmetric beam profile compared to that of edge-emitting lasers. This makes it easy to collimate the output beam with a simple optical element. Also, VCSELs have 3-dB communication bandwidth as large as 20 GHz [4]. These advantages make VCSEL an ideal choice as the optical signal source for long-distance transmission.

In the receiver photodiodes (PD) are typically used due to their high bandwidth and linear response. The most common types of PD used in LiFi technology are positive-intrinsic-negative (PIN) PDs and avalanche photodiodes (APDs). However, PDs can require additional power to generate the sometimes high bias voltage. Therefore, solar cells can be a good energy-neutral alternative to photodiodes (PDs) as they can convert variations in the intensity of the light to electrical signals without the application of reverse bias voltage. Furthermore, solar panels are by default manufactured with multiple solar cells connected in series and parallel configuration. This results in a large active area as a communication receiver and increases the energy harvesting capability. The optical energy harvested by a solar panel can be used to offset the energy consumed by the rest of the

Manuscript received April 2, 2021; revised June 15, 2021; accepted July 5, 2021. Date of publication July 14, 2021; date of current version October 4, 2021.

Sovan Das is with LiFi Research and Development Centre, University of Strathclyde, Glasgow G1 1RD, U.K., and also with the University of Edinburgh, Edinburgh EH8 9YL, U.K. (e-mail: sovan.das@ed.ac.uk).

Adrian Sparks, Enrique Poves, and Stefan Videv are with the LiFi Research and Development Centre, University of Strathclyde, Glasgow G1 1RD, U.K. (e-mail: adrian.sparks@strath.ac.uk; enrique.poves@strath.ac.uk; stefan.videv@strath.ac.uk).

John Fakidis is with the Microsoft Research, Cambridge CB1 2FB, U.K. (e-mail: v-ifakidis@microsoft.com).

Harald Haas is with the University of Strathclyde, Glasgow G1 1RD, U.K. (e-mail: harald.haas@strath.ac.uk).

Color versions of one or more figures in this article are available at https://doi.org/10.1109/JLT.2021.3096734.

Digital Object Identifier 10.1109/JLT.2021.3096734

components of the communication system. Also, the large active area of the solar panel relaxes the process of alignment between transmitter and receiver (at long distances). Conventional PDs have a small area and can be very difficult to align when used for long-distance communication.

This paper discusses the effects and trade-offs when a solar panel is used simultaneously for energy harvesting and communication. The simultaneous energy harvesting and communication performance of a solar panel has been maximized using the proposed solar panel receiver circuit structure. The effect of sunlight on the communication performance of a solar panel as an OWC receiver is studied and estimated using an equivalent circuit model of a solar panel. The variation in frequency response and signal-to-noise ratio (SNR) is estimated for varying solar irradiance. An experimental setup was developed to verify the estimations from the equivalent circuit model. In the experiment, the maximum user available data rate with full networking capabilities achieved by the system is 28.3 Mb/s over a distance of 3.5 m, while it was able to simultaneously harvest energy using the maximum power point tracking (MPPT) [5] technique. The peak power that could be harvested from the solar irradiation is 4.5 W with a 5 W silicon (Si) solar panel, and the harvested energy is stored in a 38 Wh lithium-ion (Li-ion) battery. The variation in data rate and energy harvesting is shown for different solar irradiances. The experiment was conducted for a link of distance 3.5 m only because the main goal of this paper is to study the effects of the sunlight on the communication performance of the solar panel rather than the maximum link distance.

The rest of this paper is organized as follows: in Section II all the experiments and models of solar panels as OWC receivers developed previously are discussed and reviewed. Section III describes the equivalent circuit model of the solar cell used in this paper and highlights the key parameters of the model that determines the energy harvesting and communication performance of a solar cell. In Section IV the effects of varying sunlight conditions on the communication performance of the solar cell model are studied. Section V discusses the experimental setup and the system deployed in order to verify the estimations and simulations. In Section VI the results are shown and discussed. And in Section VII the concluding remarks of the paper are presented.

## II. Background

Solar cells have traditionally been developed to harvest energy directly from sunlight and relatively little investigation has been carried out into their use as an optical data receiver with simultaneous energy harvesting. There are several types of solar cells and choosing the appropriate technology can be difficult for simultaneous energy harvesting and communication applications. Solar panels can be differentiated based on the type of semiconductor junction and material used, but they are commonly classified by generation. Single-junction and multi-junction solar cells differ in the number of layers that capture the sunlight, whereas the classification by generation emphasizes the materials and efficiency of the different types of solar cells that make up a panel. The first generation of solar panels is based on Si solar cells. They are widely used for energy harvesting due to their low manufacturing cost. They are further divided into two categories: polycrystalline and monocrystalline [6]. The latter has higher efficiency and has better temperature stability than the former. Using a first-generation solar panel as an OWC receiver relaxes the strict alignment requirement and the need for complex optical elements on the receiver side as they have a large active area. These solar panels are also low-cost, easily available, and are commonly deployed for large-scale solar energy harvesting.

In this work, we have considered a first-generation solar panel as this knowledge can be used to upgrade the existing solar energy harvesting systems. These are most commonly based on first-generation solar panels, due to the easy availability of silicon and its low manufacturing cost. Furthermore, this study can be extended to later generations of solar panels as they operate on the same underlying principles. There have been several studies using solar panels as an OWC receiver. Table I. presents a comparison of the published figures for simultaneous data communication and energy harvesting performance in PV OWC systems. In such systems, solar panels are meant for both power harvesting and data communication. Therefore, the product of the harvested power and the data communication rate has been used as a figure of merit. In this work, this product of the simultaneous power harvested and the data communication performance has been maximized for a first-generation Si-PV panel. These first-generation solar panels were never developed or designed to be used as OWC receivers. Therefore, the electrical characteristics of the panel relevant to communication such as linearity, speed of response, sensitivity to the incident optical signal, and temperature stability have been investigated in. In a data rate of 74 Mb/s has been demonstrated over a distance of 2 meters using a polycrystalline solar panel, and in a communication distance of 30 meters has been achieved with a maximum data rate of 8 Mb/s with full networking capabilities. These publications have not modelled the effects of simultaneous energy harvesting and communication, and only consider the communications performance of the solar panel OWC receiver. The following sections show how important it is to understand the trade-off between data communication and energy harvesting when both are carried out simultaneously.

## III. Principles of Operations and Modelling

To understand the effects of simultaneous energy harvesting on the data communication performance, an equivalent circuit model of a solar panel needs to be considered. We aim to create a circuit model that is electrically equivalent and is based on discrete ideal electrical components, whose behavior is well defined analytically.

### *A. Energy Harvesting & Simultaneous Communication Model*

Generally, a single diode model is used to represent a solar cell as used in [7]–[16]. The single diode model structure is identical to the structure shown in Fig. 1 without the dashed line components. Furthermore, a solar panel interfacing circuit

TABLE I
OWC LINKS USING PV CELLS WITH SIMULTANEOUS ENERGY HARVESTING

| Ref. | Active Area ($cm^2$) | Modulation Technique | Communication Bandwidth used (MHz) | Distance (m) | Maximum Data Rate (Mb/s) | Maximum Power Harvesting (W) | Product of Simultaneous Power Harvested and Data Rate (WMb/s) |
|---|---|---|---|---|---|---|---|
| This work | 667.08 | DCO-OFDM | 16 | 3.5 | 28.1** | 4.5## | 28.53 |
| [7] | 4 | DCO-OFDM | 2.77 | 0.4 | 363* | 0.01## | 3.63 |
| [8] | 432 | DCO-OFDM | 2 | 0.95 | 11.84* | 0.11## | 1.3024 |
| [9] | 0.008 | DCO-OFDM | 237.2 | 2 | 784* | 0.001## | 0.784 |
| [10] | 7.29 | - | - | 0.4 | 0.003* | 1## | 0.003 |
| [11] | 7.5 | DCO-OFDM | 4 | 2 | 15.03* | - | - |
| [12] | 667.08 | DCO-OFDM | 5 | 30 | 8** | 4.1# | - |
| [13] | 432 | DCO-OFDM | 0.35 | 0.39 | 7.01* | - | - |
| [14] | 26.05 | QAM-OFDM | 0.4 | - | - | 0.446## | - |
| [9] | 0.008 | DCO-OFDM | 237.2 | 2 | 1041* | Short-circuit mode | - |
| [15] | 667.08 | DCO-OFDM | 22 | 2 | 74.03* | Short-circuit mode | - |
| [16] | - | PAM-DMT | 9 | 0.1 | 17.05* | Reverse-biased mode | - |

*Offline processing without networking headers
**Real-time traffic with TCP/IP headers
# Claimed based on the capability of the PV
## With simultaneous data communication

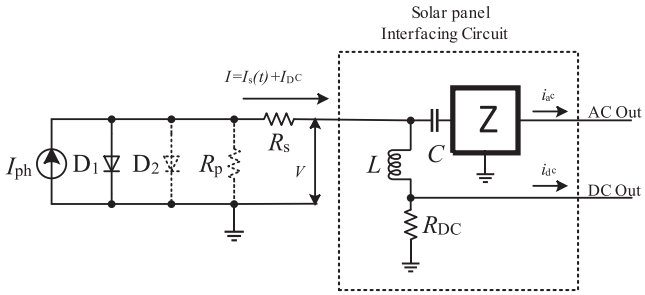


Fig. 1. PV cell model with an interfacing circuit.

is also shown in Fig. 1. In this paper, the single diode model is not considered because the single diode equation assumes a constant value for the ideality factor *n*, as studied previously in [7]–[16]. In [17], both the single diode model and double diode model of a PV was compared to study the energy harvesting parameters. In this work, the double diode model has been used to study the both the communication characteristics and simultaneously the energy harvesting performance of a solar panel. Using an accurate equivalent circuit model for the PV enables extending this work to other generations of PV cells such as organic PV cells, GaAs-based PV cells, multi-junction PV cells, *etc*. The electrical circuit parameters such as diode voltage, diode capacitance, internal resistance and current density will vary for each type of PV cell used in the system, based on the manufacturing technique and semi-conductor used in the PV cell. In reality, the ideality factor is a function of the voltage across the device [17]. At high voltages, when the recombination at the junction in the device is dominated by the surface and the bulk regions, the ideality factor is close to one, which is represented by the diode $D_1$. However, at lower voltages recombination in the junction dominates and the ideality factor approaches two. In this paper, the communication performance will be evaluated under varying solar irradiation and this will cause the voltage across the PN-junction to vary significantly. Therefore, the ideality factor needs to be considered for accurate modeling. The junction recombination is modeled by adding a second diode, which is depicted with a dashed line in Fig. 1. The ideality factor for this second diode is typically set to two [17]. Therefore, the total current generated by the solar cell is represented as *I* and defined by using Schottky's diode equation as shown in (1), where $I_{\rm ph}$ is the photogenerated current, $I_{\rm o1}$ is the diode saturation current for $D_1$, $I_{\rm o2}$ is the diode saturation current for $D_2$, *V* is the voltage across the solar panel, *q* is the charge of an electron, $R_{\rm p}$ is the shunt resistance, $R_{\rm s}$ is the series resistance, *k* is the Boltzmann's constant, and *I* is the sum of alternating current (AC) generated due to the received optical signal and the direct current (DC) generated due to the solar irradiation. Therefore $I = I_{\rm s}(t) + I_{\rm DC}$, where $I_{\rm s}(t)$ is the AC signal component and $I_{\rm DC}$ is the DC signal component.

$$I = I_{\rm ph} - I_{\rm o1}\left[e^{\frac{q(V+IR_{\rm p})}{kT}} - 1\right] - I_{\rm o2}\left[e^{\frac{q(V+IR_{\rm p})}{2kT}} - 1\right] - \frac{V + IR_{\rm s}}{R_{\rm p}} \tag{1}$$

In (1) the subtraction by 1 in the square bracket terms can be ignored for approximation, which makes the analysis easy. This is because the exponential terms give values typically much

larger than 1 [17]. Therefore, (1) can be further simplified to (2).

$$= I_{\rm ph} - I_{\rm o1}\left[e^{\frac{q(V+IR_{\rm p})}{kT}}\right] - I_{\rm o2}\left[e^{\frac{q(V+IR_{\rm p})}{2kT}}\right] - \frac{V+IR_{\rm s}}{R_{\rm p}} \tag{2}$$

$I_{\rm ph}$ in (2) represents the generated photocurrent. When there is no photocurrent generation $I_{\rm ph} = 0$ and the solar panel will act as a passive load. Therefore, the dark current for the panel can be denoted as shown in (3) [17].

$$I_{\rm D} = I_{\rm o1}\left[e^{\frac{q(V-IR_{\rm p})}{kT}}\right] + I_{\rm o2}\left[e^{\frac{q(V-IR_{\rm p})}{2kT}}\right] + \frac{V-IR_{\rm s}}{R_{\rm p}} \tag{3}$$

### *B. Noise Analysis*

Solar panels convert an incident optical power $P_{\rm s}$ into an electric current *I* using the photovoltaic effect. In the photovoltaic effect, $P_{\rm s} \propto I$ which implies $I = \mathcal{R}P_{\rm s}$ where $\mathcal{R}$ is a constant at a given wavelength and is defined as the responsivity of the material of which the solar cell is made. The relation $I = \mathcal{R}P_{\rm s}$ is valid only if the *I* is interpreted as the average current generated. However, this is not the case for an ideal optical receiver. The four noise mechanisms (thermal noise, shot noise, dark current noise, and input noise) need to be considered to understand the effects of simultaneous energy harvesting and communication performance.

Thermal noise, also known as Johnson noise, follows a Gaussian distribution and can be characterized by its constant power spectral density given in (4), where $Z_{\rm L}$ is the load impedance, and *T* is the absolute temperature. The unit of ${\sigma_{\rm th}}^2$ is W/Hz. For the solar panel as a receiver with communication bandwidth *B*, the mean-square noise current representing the total thermal noise power can be expressed as $\langle i_{\rm th}^2 \rangle$ and is defined in (5).

$$\sigma_{\rm th}^2 = \frac{4kT}{|Z_{\rm L}|} \tag{4}$$

$$\langle i_{\rm th}^2 \rangle = \sigma_{\rm th}^2\, B \tag{5}$$

Shot noise is white, therefore a Gaussian distribution can be used to define the shot noise statistics. The shot noise power spectral density ${\sigma_{\rm sh}}^2$ can be expressed as in (6), where *I* is the photocurrent as shown in Fig. 1 and *q* is the electron charge. As $I = \mathcal{R}P_{\rm s}$, ${\sigma_{\rm sh}}^2$ can alternatively be defined by the responsivity and total optical power received as shown in (6). The mean-square noise current $\langle i_{\rm sh}^2 \rangle$ for the interested bandwidth is shown in (7).

$$\sigma_{\rm sh}^2 = 2qI = 2q\mathcal{R}P_{\rm s} \tag{6}$$

$$\langle i_{\rm sh}^2 \rangle = \sigma_{\rm sh}^2\, B \tag{7}$$

Dark current noise is the constant current that exists when no light is incident on the solar panel. The dark current noise can also be treated as white noise with Gaussian distribution, because the statistical nature of the charge carrier generation process is similar to that discussed for the shot noise. For $I_{\rm D}$ from (3), the noise power spectral density ${\sigma_{\rm D}}^2$ is defined in (8). The dark current noise power $\langle i_{\rm D}^2 \rangle$ for the selected bandwidth *B* can be expressed as shown in (9).

$$\sigma_{\rm D}^2 = 2qI_{\rm D} \tag{8}$$

$$\langle i_{\rm D}^2 \rangle = \sigma_{\rm D}^2\, B \tag{9}$$

The optical signal is converted to current by a solar panel, but for further processing in the communication chain, the time-varying photocurrent signal needs to be converted to electrical voltage. An electrical trans-impedance amplifier is used to amplify the photocurrent signal and convert it to voltage. Noise generated by the first stage of the amplifier must also be considered in the receiver Signal-to-Noise Ratio (SNR) analysis because the amplifier noise power is comparable to the electrical signal power fed to the amplifier. The trans-impedance gain $Z_{\rm amp} = v_{\rm out}/i_{\rm ac}$, where $i_{\rm ac}$ is the input signal current as depicted in Fig. 1 and $v_{\rm out}$ is the output signal voltage from the amplifier. The output voltage error $v_{\rm amp}$ is the output voltage from the amplifier when the input signal current is zero. This parameter is generally provided by the manufacturer of the operational amplifier in the corresponding datasheet. Henceforth, the output noise power from the amplifier is defined as $\langle v_{\rm amp}^2 \rangle$ and the input noise power $\langle i_{\rm amp}^2 \rangle$ can be calculated using (10).

$$\langle i_{\rm amp}^2 \rangle = \frac{\langle v_{\rm amp}^2 \rangle}{Z_{\rm amp}^2} \tag{10}$$

Under real-world conditions, many communication devices are transmitting and receiving signals simultaneously and every wire connecting an optical receiver to the subsequent stages can be considered as an antenna. These radio frequency (RF) signals can be picked up unintentionally by the wires and terminals which create interference with the signal of interest. This problem is solved by creating a Faraday cage around the exposed terminals and wires. Therefore, for the noise estimation purpose, the interference and noise due to RF can be approximated to zero.

## IV. Estimation of Communication Parameters

For an optical communication receiver, there are three main factors on which the communication performance will depend, namely spectral responsivity, frequency response, and noise performance. As a first-generation Si-based solar panel is used in this work, the optical to electrical energy conversion, *i.e.,* spectral responsivity, of Si peaks at around 1000 nm [6]. By choosing the appropriate optical signal transmitter's wavelength the optical to electrical signal conversion at the solar panel can be maximized. Next, the bandwidth and noise performance of the solar panel will depend on how the panel is interfaced with the subsequent stages of the communication system. As it can be seen in Section III-B, the thermal noise power is inversely proportional to the load impedance $Z_L$, and a large load impedance magnitude helps reduce the thermal noise. However, as investigated in and an increase in load impedance would reduce the communication bandwidth. The best communication bandwidth is achieved under a short-circuit condition. On the contrary, for energy harvesting purposes short-circuit conditions would generate no power as the voltage is zero. To overcome this issue the solar panel interfacing circuit is designed as shown

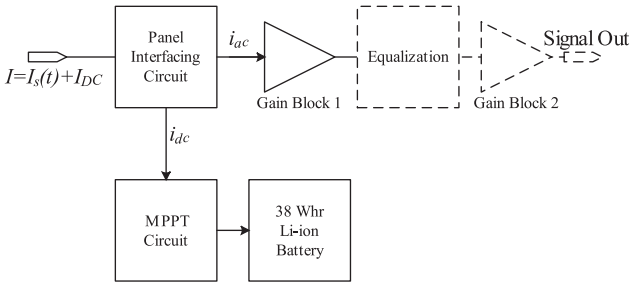


Fig. 2. Receiver circuit functional block diagram.

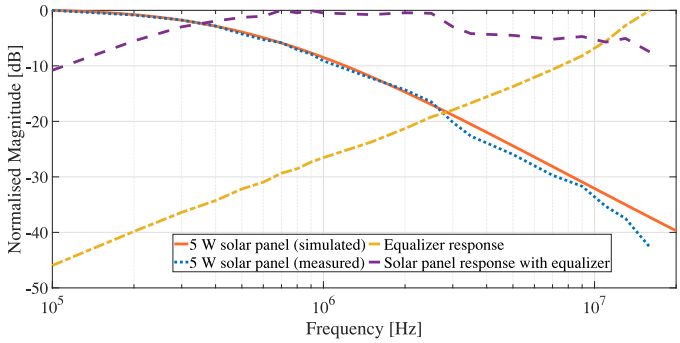


Fig. 3. Solar panel bandwidth.

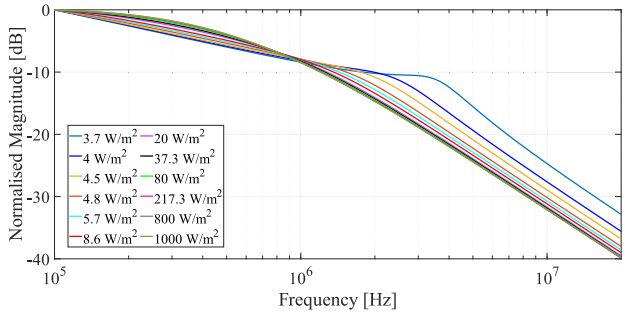


Fig. 4. Frequency response for varying solar irradiance.

in Fig. 1 so that the inductor $L$ and capacitor $C$ separate the DC and AC components of the signal. The DC Out terminal is then connected to an MPPT circuit which holds the voltage constant and non-zero across the panel ensuring that the communication bandwidth achieved is as large as possible. The MPPT circuit design is taken from the Texas Instruments reference design for the battery charge controller for solar power described in [18]. The impedance network $Z$ in the interfacing circuit is a resistor-inductor-capacitor resonant circuit whose bandwidth is equal to the chosen communication bandwidth $B$. In this case, $R_{\mathrm{DC}}$ is 5.1 kΩ, $C$ is 100 nF and $L$ is 150 nH, as $B$ is 16 MHz. This ensures the undesired low and high frequencies are filtered out and the effective impedance across the panel is only resistive with a low value.

### A. *Frequency Response of a Solar Panel*

Using the equations (2),(3), (11)–(14) and the equivalent circuit models discussed in Section III, the frequency response of the panel was simulated using TINA-TI [19], which is a simulation program with integrated circuit emphasis (SPICE). The simulation was carried out with the receiver circuit structure as shown in Fig. 2 without the components depicted with dashed line. In the simulation, the temperature was kept constant at 298 K.

$$C_{\mathrm{d}} = \frac{k\tau_{\mathrm{n}} I_{\mathrm{d}}}{T} \tag{11}$$

$$R_{\mathrm{s}} = \left(\frac{P}{P_{\mathrm{MP}}} + 1\right)\frac{V_{\mathrm{oc}}}{I_{\mathrm{sc}}} \tag{12}$$

$$R_{\mathrm{p}} = \left(\frac{P_{\mathrm{MP}}}{P + P_{\mathrm{MP}}}\right)\frac{V_{\mathrm{oc}}}{I_{\mathrm{sc}}} \tag{13}$$

The diffusion capacitance, series and shunt resistances were defined by the equations as shown in (11)–(13). In equation (11) $C_{\mathrm{d}}$ is the diffusion capacitance [20], $k$ is the Boltzmann's constant, $I_{\mathrm{d}}$ is the current through the diode, $\tau_{\mathrm{n}}$ is the minority carrier lifetime which is defined in detail in and $T$ is the temperature. The diffusion capacitance for $\mathrm{D}_1$ and $\mathrm{D}_2$ is estimated separately for each diode using this equation. Furthermore, the series resistance is defined in equation (12) [21] where $P$ is the power harvested for the incident optical power, $P_{\mathrm{MP}}$ is the maximum power that can be harvested by the panel, which is 5 W in this case, $V_{\mathrm{oc}}$ is the open-circuit voltage across the panel and $I_{\mathrm{sc}}$ is the short-circuit current. The open-circuit voltage and short-circuit current of the solar panel used in this case was 22 V and 330 mA, respectively [22]. Similarly, the shunt resistance $R_{\mathrm{p}}$ is defined in equation (13).

The receiver structure shown in Fig. 2 was implemented in practice and the frequency response simulation was verified experimentally. The simulated and measured frequency response of the solar panel is shown in Fig. 3. From Fig. 3 it can be inferred that the simulated double-diode model matches the response in terms of communication performance to the solar panel chosen in practice. Henceforth, the short-circuit current for the solar panel was measured by varying the incident optical power. A 1 kW PAR64 halogen lamp [23] with a 0.8 kW halogen bulb was used as a sunlight emulator. The color temperature of the halogen lamp was 3200 K, although the color temperature of sunlight on the surface of the earth on a bright sunny day is around 5700-6000 K [24]. Therefore, a color filter [25] was used in front of the halogen lamp set up to produce a light spectrum equivalent to the spectrum of sunlight. The halogen lamp was used with a parabolic reflector to concentrate the beam onto the 667 cm$^2$ active area of the solar panel and a dimmer was used to control the light output from the halogen lamp. The halogen lamp was placed at a distance of 60 cm from the solar panel such that the maximum intensity measured with a lux meter on the panel is approximately 130000 lux. Using the solar irradiance to lux illuminance conversion factor of 0.0079 W/lux [26] the emulated solar irradiance on the solar panel was calculated, and the maximum value was 1000 W/m$^2$. Then the short-circuit solar panel current is measured while varying the emulated solar irradiance using the dimmer and this is plotted in Fig. 5. The short-circuit current measured is approximately equal to $I_{\mathrm{ph}}$, as $R_{\mathrm{s}}$ is less than 1 Ω. Furthermore, using this short-circuit current as $I_{\mathrm{ph}}$ the frequency response for different solar irradiance was

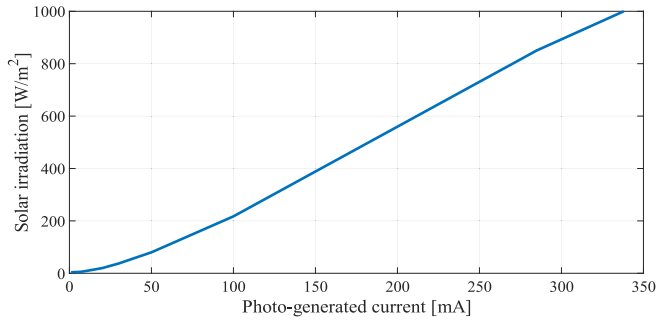


Fig. 5. Photo-generated current for varying solar irradiance.

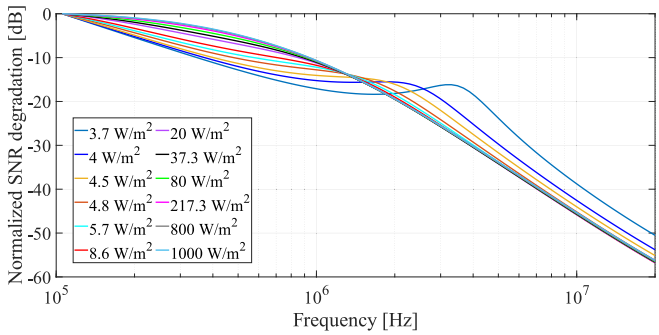


Fig. 6. Estimated SNR degradation for varying solar irradiance.

simulated and verified experimentally. Fig. 4 shows the variation in frequency response due to the variation in solar irradiance with the receiver circuit as depicted in Fig. 2. This variation in frequency response occurs due to the constant voltage held across the panel by the MPPT circuit. As the voltage across the panel is constant, the generated photocurrent is varying due to variations in the incident optical intensity. The internal effective resistance of the panel is varying due to changes in the photocurrent, which results in the variation of the time-constants of $D_1$ and $D_2$. The time-constants of $D_1$ and $D_2$ are directly related to the communications bandwidth of the solar panel.

### *B. Estimation of SNR*

The next important parameter which determines the performance of the solar panel as a communication receiver is SNR. When OFDM is used, the magnitude of the SNR of the frequency subcarriers determines the modulation order that could be used over the selected communication bandwidth for a given bit error rate. The SNR for the received signal was calculated using the simulation results and equation (14) obtained from TI-TINA in MATLAB for the solar panel model discussed in Section III. In Fig. 6 the normalized SNR for the received signal is plotted for different values of emulated solar irradiance incident on the panel. The SNR estimated in Fig. 6 depicts the degradation introduced by the solar panel during the optical to electrical signal conversion.

$$\mathrm{SNR} = \frac{\langle I_{\mathrm{s}}^2(t)\rangle}{\langle i_{\mathrm{th}}^2\rangle + \langle i_{\mathrm{sh}}^2\rangle + \langle i_{\mathrm{D}}^2\rangle + \langle i_{\mathrm{amp}}^2\rangle} \tag{14}$$

In Fig. 6 the SNR increases at the lower frequencies with the increase in emulated solar irradiance on the solar panel. This

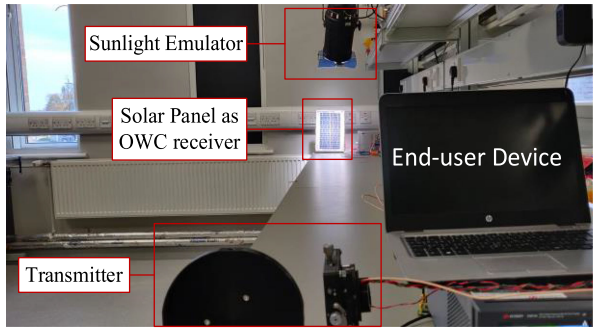


Fig. 7. Experimental setup.

can be explained by the reduction of the diode resistances of $D_1$ and $D_2$ due to an increase in the photogenerated current. At higher frequencies, the reduction of SNR with an increase in optical intensity can be explained by the increase in shot and thermal noise. As seen in equations (6) and (7) the shot noise increases with the increase in total optical incident power $P_{\mathrm{s}}$. In the case of thermal noise, the solar spectrum consists of both long and short IR radiation. This IR radiation will generate heat in most of the materials as the molecules resonate with the IR wavelength. Therefore, an increase in temperature $T$ in equation (4) results in an increase in the thermal noise. Furthermore, the SNR plots for each solar irradiance follows the same trend as the frequency response, shown in Fig. 4. On the contrary, the dark current noise and the amplifier input noise are constant for the varying optical intensity as they are independent of the optical power incident and the temperature of the solar panel. Therefore, the estimations in this section show that there is a trade-off in communication performance when the solar panel is used simultaneously for harvesting solar energy.

## V. Experimental Setup

In order to verify the estimations obtained in Section IV, it is necessary to evaluate the trade-off between energy harvesting and simultaneous communication. A real-time optical link with full networking capability is developed as shown in Fig. 7. To establish a real-time link with full networking capability a full-duplex link is required. In this setup, the downlink is the optical link, and the uplink is realized using a coaxial cable. The transmitter is based on the design developed in [12]. The transmitter uses an off-the-shelf 940 nm VCSEL as the optical source and the beam is collimated using a commercially available off-axis parabolic mirror. The transmitter is classified as class 1M and the VCSEL is driven by a current driver with a 3 dB communication bandwidth of 65 MHz [12]. The receiver circuit consists of an analog equalizer which flattens the frequency response of the solar panel up to 16 MHz, shown in Fig. 3. The proposed solar panel interfacing circuit, as discussed in Sections III and IV, and the equalizer circuit are integrated into the receiver circuit design in order to enable the energy harvesting capability of the solar panel. The overall receiver circuit structure is shown in Fig. 2. As the receiver design includes an analog equalizer stage this helped in increasing the usable communication bandwidth of the solar panel to 16 MHz. In the MPPT circuit, the solar panel voltage

TABLE II
PHYSICAL LAYER SPECIFICATION

| | |
|---|---|
| Channel bandwidth | 16 MHz |
| Subcarrier Spacing (Δf) | 250 KHz (16 MHz/64 Pt FFT) |
| Modulation | BPSK, QPSK, 16QAM, 64QAM |
| Coding Rate | ½, ⅔, ¾ |
| FFT Period ($T_{FFT}$=1/Δf) | 4 µs |
| Cyclic Prefix duration ($T_{GI2}$ = $T_{FFT}$/2) | 2 µs |

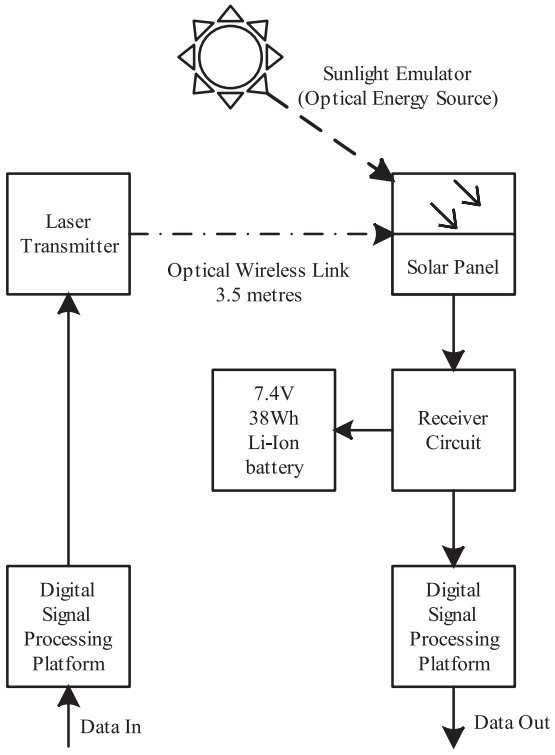


Fig. 8. System functional setup.

needs to be adjusted. In this work, the voltage was set to 7.22 V, which is the nominal voltage *i.e.,* maximum power point as recommended by the manufacturer [22]. The harvested energy is stored in a Lithium (Li)-ion battery with a capacity of 38 Wh. For digital signal processing (DSP) an application-specific integrated circuit (ASIC) from pureLiFi [27] is used, which is based on the IEEE 802.11 wireless local area network (WLAN) standard [28]. The specification of physical (PHY) layer used in the experiment is shown in Table II. In IEEE 802.11 WLAN standard, OFDM is used primarily to utilize the channrl bandwidth efficiently. There are several variants in OFDM employed in optical communication such as Asymmetrically Clipped Optical OFDM (ACO-OFDM) [29], Enhanced unipolar OFDM (eU-OFDM) [30], DC-biased optical OFDM (DCO-OFDM) [31], *etc*. In this experiment, the system uses DCO-OFDM, as with lower system complexity higher spectrally efficiency could be achieved compared to the other mentioned OFDM variants. The functional block diagram and the interconnection of each sub-system is shown in Fig. 8. As the DSP platform, *i.e.,* the pureLiFi ASIC, provides only the functionality of the PHY layer

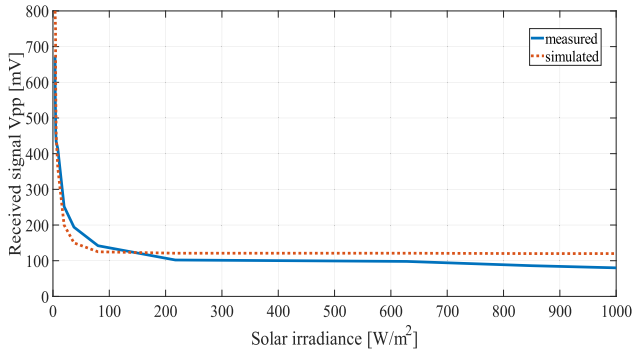


Fig. 9. Received signal power variation due to varying solar irradiation.

and lower medium access control (MAC) layer, a host processor is needed to implement the remaining three layers, *i.e.,* network, transport, and application layer of the transport control protocol and internet protocol (TCP/IP) network stack. Laptops on either end of the communication nodes were used as the host processor as well as the end-user device. To simulate real-time network traffic and measure the network bandwidth, iPerf [32] is used on the end-user devices. Using iPerf, the network bandwidth was measured at a constant optical intensity incident on the panel for 50 s and the average data rate was recorded. This process was iterated with different emulated solar irradiance ranging from 0 W/m$^2$ to 1000 W/m$^2$ using the procedure as discussed in Section III-B. The data rate was measured up to 1000 W/m$^2$ as that is the nominal solar irradiation measured on the surface of the earth during a bright sunny day. Simultaneously, the DC voltage and current generated by the solar panel and the signal power at the receiver circuit output is recorded for different optical intensity incident on the solar panel. The recorded data is plotted and discussed further in Section VI. Furthermore, a transmitted data packet from the DSP platform was captured using an oscilloscope. The captured data packet was used to simulate the double-diode model along with the whole receiver circuit in TI-TINA to estimate the signal power at the receiver output against the varying optical power. These simulated results are compared with the experiment results and discussed further in the following section.

## VI. RESULTS & DISCUSSIONS

The experiment was successfully conducted, and the obtained results are shown in Fig. 9 and Fig. 10. The highest data rate achieved between the two end-user devices is 28.3 Mb/s while harvesting no power. Alternatively, the peak power harvested with a 5 W solar panel at the equivalent illumination of the sun on a bright sunny day is 4.5 W simultaneously with a data rate of 6.34 Mb/s between the two end-user devices. Fig. 9 shows the received data signal power variation against the varying solar irradiation for both the simulated model and the experimental setup. The results from the simulated model align with the results from the experimental setup. Therefore, it can be inferred that the simulated model matches the experimental setup. The exponential decrease in the received signal power with the increase in solar irradiance follows the trend shown

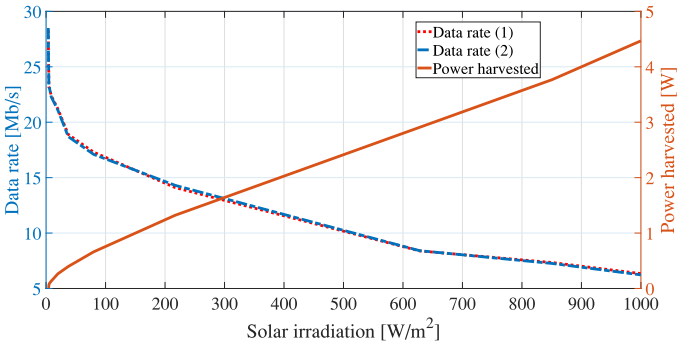


Fig. 10. Variation in data rate with simultaneous energy harvesting.

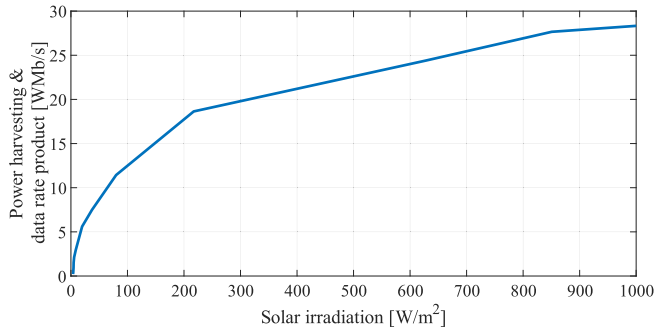


Fig. 11. Simultaneous power harvesting and data rate performance.

by the reduction in frequency bandwidth when the emulated solar irradiance is increased in Fig. 4. In Fig. 10 the variation in data rate along with the power harvested from the solar panel is shown against the variation in solar irradiation. The decrement in data rate with the increase in solar irradiance follows the same trend as the frequency response and SNR as shown in Fig. 4 and Fig. 6. From this plot, it can be seen that there is a trade-off between communication and solar energy harvesting when a solar panel is used simultaneously for both. At 240 W/m$^2$ solar irradiance, there is an intersection of the data rate achieved and energy harvested simulation. At this point, the achieved data rate is 13.7 Mb/s and 1.6 W of power is simultaneously harvested. The achieved data rate is not as high as that in [15] as the highest order of modulation used by the ASIC in this experiment is 64-quadrature amplitude modulation (QAM) at ¾ code-rate under ideal conditions, while in [15] the maximum achieved modulation order was 512-QAM at ½ code rate and used offline processing on MATLAB. Also, the raw throughput measured in [15] is 74 Mb/s which neglects the bits occupied by the TCP/IP headers. The equivalent raw throughput for the setup in this paper is 37.63 Mb/s without the full networking stack overheads. The aim of this study was to investigate the effects of sunlight on a single Si-based PV when used as an OWC receiver and maximize power harvesting and data communication. Therefore, the product of two key parameters needs to be maximized. In Fig. 11, the product of power harvested, and the data rate achieved for a given solar irradiance is shown. It can be seen that with the increase in solar irradiance the product also increases. Furthermore, depending on the application, the data rate or energy harvesting capability can be maximized by choosing the appropriate voltage setting in the MPPT controller. Setting the voltage at a lower value will result in better communication performance as seen previously in [15] and a reduction in the energy harvested. Setting the voltage equal to the nominal voltage of the solar panel will achieve maximum energy harvesting, as shown in this paper, but resulting in reduced communications performance.

## VII. Conclusion

In this paper, a trade-off between energy harvesting and communication performance when an off-the-shelf Si-based solar panel is used as an OWC receiver is shown. Moreover, a receiver circuit structure has been proposed which enables to maximize the simultaneous energy harvesting and data communication performance of a PV in an OWC system. The product of solar power harvested, and data rate achieved has been maximized up to 28.53 WMb/s. Using the receiver circuit, the performance of a solar panel for power harvesting and data communication in an OWC system has been enhanced 9 times than the previously published state of the art. Additionally, the proposed receiver structure could be used for other generation of PV cells to maximize the performance as the design and estimation is based on a more accurate PV circuit model. Additionally, the simulated estimations using the PV circuit model has been verified experimentally to show the accuracy. Furthermore, depending on the application's requirements, either communication or energy harvesting performance can be maximized with the appropriate settings. Moreover, this invites future work where smart software can be developed, which controls the settings continuously during the system operation while monitoring the daylight conditions, energy requirements, and user-throughput requirements to provide an optimal experience for the end-user.

## Acknowledgment

The work of H. Haas was supported in part by Engineering and Physical Sciences Research Council under Established Career Fellowship Grant EP//1, in part by Wolfson Foundation and Royal Society.

## References

[1] L. M. Fraas, *Low-Cost Solar Electric Power*, Switzerland: Springer, 2014.
[2] J. Lin, W. Yu, N. Zhang, X. Yang, H. Zhang, and W. Zhao, "A survey on Internet of Things: Architecture, enabling technologies, security and privacy, and applications," *IEEE Internet Things J.*, vol. 4, no. 5, pp. 1125–1142, Oct. 2017.
[3] H. Haas, L. Yin, Y. Wang, and C. Chen, "What is lifi?," *J. Lightw. Technol.*, vol. 34, no. 6, pp. 1533–1543, Mar. 2016.
[4] K. Lear, V. Ochiai, H. Hou, B. Hammons, J. Banas and J. Nevers, "High-speed vertical cavity surface emitting lasers," in *Proc. Dig. IEEE/LEOS Summer Topical Meet.*, Montreal, 1997.
[5] J. A. B. Vieira and A. M. Mota, "Maximum power point tracker applied in batteries charging with PV panels," in *Proc. IEEE Int. Symp. Ind. Electron.*, Cambridge, 2008, pp. 202-207.
[6] Z. Hameiri, "Photovoltaics literature survey (No. 125)," *Prog. Photovolt.: Res. Appl.*, vol. 24, no. 3, pp. 405–407, 2016.
[7] I. Tavakkolnia *et al.*, "Organic photovoltaics for simultaneous energy harvesting and high-speed MIMO optical wireless communications," *Light: Sci. Appl.*, vol. 10, no. 41, 2021, Art. no. 41.
[8] Z. Wang, D. Tsonev, S. Videv, and H. Haas, "On the design of a solar panel receiver for optical wireless communication with simultaneous energy harvesting," *IEEE J. Sel. Areas Commun.*, vol. 33, no. 8, pp. 1612–1623, Aug. 2015.

[9] J. Fakidis, H. Helmers, and H. Haas, "Simultaneous wireless data and power transfer for a 1-Gb/s GaAs VCSEL and photovoltaic link," *IEEE Photon. Technol. Lett.*, vol. 32, no. 19, pp. 1277–1280, Oct. 2020.
[10] S.-M. Kim and J.-S. Won, "Simultaneous reception of visible light communication and optical energy," in *Proc. Int. Conf. ICT Convergence*, Jeju, 2013.
[11] R. Sarwar *et al.*, "Visible light communication using a solar-panel receiver," in *Proc. Int. Conf. Opt. Commun. Netw.*, Wuzhen, China, 2017.
[12] S. Das, E. Poves, J. Fakidis, A. Sparks, S. Videv, and H. Haas, "Towards energy neutral wireless communications: Photovoltaic cells to connect remote areas," *Energies*, vol. 12, no. 19, Oct. 2019, Art. no. 3772.
[13] Z. Wang, D. Tsonev, S. Videv, and H. Haas, "Towards Self-powered solar panel receiver for optical wireless communication," in *Proc. IEEE ICC Opt. Netw. Syst.*, Sydney, NSW, Australia, 2014, pp. 3348-3353.
[14] N. Lorriere *et al.*, "Photovoltaic solar cells for outdoor lifi communications," *J. Lightw. Technol.*, vol. 38, no. 15, pp. 3822–3831, 2020.
[15] S. Das, J. Fakidis, A. Sparks, E. Poves, S. Videv, and H. Haas, "Towards 100 Mb/s optical wireless communications using a silicon photovoltaic receiver," in *Proc. IEEE Glob. Commun. Conf.*, Taipei, 2020, pp. 1-6.
[16] W.-H. Shin, S.-H. Yang, D.-H. Kwon and S.-K. Han, "Self-reverse-biased solar panel optical receiver for simulataneous visible light communication and energy harvesting," *Opt. Exp.*, vol. 24, no. 22, pp. A1300–A1305, 2016.
[17] V. Tamrakar, S. Gupta, and Y. Sawle, "Study of characteristics of single and double diode electrical equivalent circuit models of solar PV module," in *Proc. Int. Conf. Energy Syst. Appl.*, Pune, 2015.
[18] Texas Instruments Inc., "High efficiency synchronous switch-mode charge controller - solar battery charger (BQ24650)," Jan. 2020. [Online]. Available: https://www.ti.com/product/BQ24650
[19] Texas Instruments Inc., "TINA-TI SPICE-based analog simulation program," Texas Instruments Inc., Accessed: Sep. 2020. [Online]. Available: https://www.ti.com/tool/TINA-TI.
[20] S. K. Sharma, D. Pavithra, G. Sivakumar, N. Srinivasamurthy, and B. L. Agrawal, "Determination of solar cell diffusion capacitance and its dependence on temperature and 1 MeV electron fluence level," *Sol. Energy Mater. Sol. Cells*, vol. 26, no. 3, pp. 169–179, 1992.
[21] M. Wolf and H. Rauschenbach, "Series resistance effects on solar cell measurements," *Adv. Energy Convers.*, vol. 3, pp. 455–479, 1963.
[22] Solar Technology International Ltd., "5 Watt solar panel kit," , Accessed: Jan. 2019. [Online]. Available: https://www.solartechnology.co.uk/pv-logic/5w-solar-panel-kit
[23] Philips Lighting, "par64 1000w 240v nsp," Philips Lighting, Accessed: Oct. 2020. [Online]. Available: https://www.lighting.philips.co.uk/prof/conventional-lamps-and-tubes/special-lamps/entertainment/dj-club/par56-and-par64/924783345504_EU/product
[24] J. F. Collins, "The colour temperature of daylight," *Brit. J. Appl. Phys.*, vol. 16, no. 6, 1965.
[25] LEE Filters, "Colour information and spectral charts for 201," Accessed: Oct. 2020, [Online]. Available: https://www.leefilters.com/lighting/colour-details.html#201&filter=cf&sort=number
[26] P. Michael, "A conversion guide: Solar irradiance and lux illuminance," *IEEE Dataport*, 2019.
[27] Purelifi, "LiFi ASIC PL0300 datasheet," Accessed: 2019. [Online]. Available: https://purelifi.com/lifi-asic/
[28] "IEEE standard for information technology—Telecommunications and information exchange between systems local and metropolitan area networks—Specific requirements - Part 11: Wireless LAN medium access control (MAC) and physical layer (PHY) specifications," IEEE Std 802.11-2016 (Revision of IEEE Std 802.11-2012), pp. 1–3534, 2016.
[29] S. Hranilovic and R. Bai, "Absolute value layered ACO-OFDM for intensity-modulated optical wireless channels," *IEEE Trans. Commun.*, vol. 68, no. 11, pp. 7098–7110, Nov. 2020.
[30] D. Tsonev, S. Videv, and H. Haas, "Unlocking spectral efficiency in intensity modulation and direct detection systems," *IEEE J. Sel. Areas Commun.*, vol. 33, no. 9, pp. 1758–1770, Sep. 2015.
[31] S. D. Dissanayake and J. Armstrong, "Comparison of ACO-OFDM, DCO-OFDM and ADO-OFDM in IM/DD systems," *J. Lightw. Technol.*, vol. 31, no. 7, pp. 1063–1072, 2013.
[32] ESnet/Lawrence Berkeley National Laboratory, "iPerf," Accessed: Sep. 2020, [Online]. Available: https://iperf.fr/

**Sovan Das** received the Bachelors of Engineering degree in telecommunication engineering from the PES Institute of Technology, Bangalore, India, in 2017. He is currently working toward the Ph.D. degree in optical wireless communication with The University of Edinburgh, Edinburgh, U.K. He is also a Development Engineer with the LiFi Research and Development Centre, University of Strathclyde, Glasgow, U.K. His primary research interests include photovoltaics as FSO receivers, LiFi, optical wireless communications, and autonomous aerial robotics.

**Adrian Sparks** received the B.Sc. degree in solid state physics from the University of Bath, Bath, U.K., and the MBA degree from the University of Essex, Colchester, U.K. He is currently an Optoelectronics Engineer with the LiFi Research and Development Centre, the University of Strathclyde, Glasgow, U.K. He is an experienced industrial research and development professional with 15 patents granted. Previously he has led the development of RF over fibre and optical fibre sensing products, which are currently sold all over the world. He started his career with Standard Telecommunications Laboratories (later Nortel Networks), Harlow, U.K., working on liquid crystal displays and designing the world's first commercially available ferroelectric display system. He moved on to work on optical fibre telecommunications and designed analog integrated circuits for the first optically amplified transatlantic cable. He worked for seven years on all optical network architecture for Nortel, Ottawa, ON, Canada and in the U.K., generating seven patent applications.

**Enrique Poves** received the M.Sc. and Ph.D. degrees in telecommunications engineering from Universidad Politécnica de Madrid, Madrid, Spain, in 2004 and 2010, respectively. After research with Universidad Politécnica de Madrid and The University of Edinburgh, Edinburgh, U.K., and six years working in industry, he is currently Applications Engineer with the LiFi Research and Development Centre, University of Strathclyde, Glasgow, U.K. His main research interests include optical wireless communications systems and modulation techniques, and the identification of use cases and applications for industry and consumer markets.

**Stefan Videv** received the B.Sc. degree in electrical engineering and computer science and the M.Sc. degree in communications, systems and electronics from Jacobs University, Bremen, Germany in 2007 and 2009, respectively and the Ph.D. degree from The University of Edinburgh, Edinburgh, U.K., in 2013 for his thesis titled Techniques for Green Radio Cellular Communications. He is currently the Director of Engineering for the LiFi Research and Development Centre. He leads industry engagement as the Director of engineering, all prototyping and development work, and driving the center's technology roadmap continued renewal and implementation. His research interests include high speed optical communications, resilient communication system design, and energy efficient communications.

**John Fakidis** received the Diploma (M.Eng.) in electrical and computer engineering from the Aristotle University of Thessaloniki, Thessaloniki, Greece, in 2011 and the Ph.D. degree for his thesis titled Optical wireless energy transfer for self-sufficient small cells from the Institute for Digital Communications, The University of Edinburgh, Edinburgh, U.K., in 2017 in collaboration with Nokia, Bell Laboratories in Ireland. He is a Postdoctoral Research Associate with Light Fidelity (LiFi) Systems, LiFi Research and Development Center (LRDC), The University of Edinburgh until 2020. He was an Optical Engineer with LRDC, University of Strathclyde, Glasgow, U.K. He is the holder of world-record data rates in simultaneous optical wireless data and power transfer. He is currently an Optical Scientist with Microsoft Research Cambridge, Cambridge, U.K.

**Harald Haas** (Fellow, IEEE) received the Ph.D. degree from The University of Edinburgh, Edinburgh, U.K., in 2001. He is currently a Distinguished Professor of mobile communications with the University of Strathclyde and the Director of the LiFi Research and Development Centre. He also set-up and co-founded pureLiFi Ltd, where he is currently the Chief Scientific Officer. He has authored more than 550 conference and journal papers. His main research interests include optical wireless communications, hybrid optical wireless and RF communications, spatial modulation, and interference coordination in wireless networks. His team invented spatial modulation. He introduced LiFi to the public at an invited TED Global talk in 2011. LiFi was listed among the 50 best inventions in TIME Magazine in 2011. He gave a second TED Global lecture in 2015 on the use of solar cells as LiFi data detectors and energy harvesters. He was the recipient of the Outstanding Achievement Award from the International Solid State Lighting Alliance in 2016, the IEEE Vehicular Society James Evans Avant Garde Award in 2019, the Royal Society Wolfson Research Merit Award in 2017 and was elevated to IEEE Fellow. In 2018, he was also the recipient of the three-year EPSRC Established Career Fellowship extension and was elected Fellow of the IET. In 2017, he was elected a Fellow of the Royal Society of Edinburgh. In 2019, he was elected Fellow of the Royal Academy of Engineering.